Role of Residual Stress in Structural Integrity Assessment of Cracked Components at Elevated Temperatures

Kamran Nikbin[1]

Abstract: Weldments and welded regions of components are likely to see failure at elevated temperatures earlier than homogenous parent material. In some cases variable loading could also introduce creep/fatigue crack growth. These weld regions not only contain variable creep properties but are likely to contain residual stresses which could relax in time. There are three key factors which may determine a successful outcome for remaining life assessment of engineering components containing residual stresses in the vicinity of welds. The first is standardized testing and measurement procedures. The second is the development of appropriate and accurate correlating parameters to treat the results in a unified and verifiable manner in order to produce 'benchmark' material crack initiation and growth properties of weldments. The third is the development of accurate and verifiable models for life assessment of welded components. A short review of available fracture based life assessment codes is presented followed by the description of the correlating parameters employed in fracture based analyses of components at high temperatures. The paper highlights new testing, measurement and predictive procedures which are needed for less conservative life assessment methodologies. The important points relating to the creep crack growth behaviour of weldment specimens, residual stress measurements and modelling of residual stresses are identified. The methodologies are presented and examples of the analysis techniques are applied to feature size components.

Keyword: creep damage; fracture mechanics; residual stress; life assessment; crack growth; component

1 Introduction

The power generation industry is striving to meet criteria for clean and sustainable energy production by increasing efficiency while simultaneously decreasing levels of chemical emissions and pollutants. The efficiency of conventional steam and gas turbine power plant can be significantly improved by increasing the operating temperature, leading to reduced fuel consumption and lower levels of harmful emissions. With the trend towards higher operating temperatures and the competing need to extend the life of existing power plant, more accurate and reliable experimental data for use in improved predictions of component lifetimes at elevated temperatures are needed. Early codes [1-2] recommended life assessments techniques for uncracked bodies. However life prediction methods using fracture mechanics methods has since dominated. However most of the work has been tailored around parent materials which have homogenous creep properties. Very little has been done in weldments which are likely the sited where failure would occur the earliest. Lack of information on weldments has bee due to the complicated nature of the microstructure and the varying material properties. This paper therefore discusses the developments relating to the behaviour of cracks in components operating at elevated temperatures which contain welds.

1.1 Background to Life Assessment Codes

Components in the power generation and petrochemical industry operating at high temperatures are almost invariably submitted to static and/or combined cycle loading. The alloys used can vary between low carbon steels to high chrome superalloys with various alloying contents. In addition

[1] Mechanical Engineering Department, Imperial College, London, SW7 2AZ, UK.

these components have welded parts which will have different alloying and microstructural properties. The failures can be due to large deformations, creep rupture and/or crack growth. The development of codes in different countries has moved in very similar direction and in many cases the methodology has been borrowed from a previously available code in another country. Early approaches to high temperature life assessment have used methodologies based on defect-free assessment codes. For example ASME Code Case N-47 [1] and the French RCC-MR [2], which have many similarities, are based on lifetime assessment of un-cracked structures. More recent methods make life assessments based on the presence of defects in the component. The more advanced codes dealing with defects over the range of creep and creep/fatigue interaction in initiation and growth of defects are the BS 7910 [3], British R5/R6 [4,5], the API RP 579 [6] and the French A16 [7] which have clear similarities in terms of methodology. It is also obvious from these assessment methods that the correct evaluation of the relevant fracture mechanics parameters, for which the lifetime prediction times are dependent upon, are extremely important.

It is also evident that the detailed calculation steps, which are proposed in these documents alone, do not improve the accuracy of the life prediction results. In any event as these procedures have been validated for limited sets of geometries and 'Benchmark' material data, their use in other operating conditions will need careful judgment. These aspects have been considered in codes [8,9] in order to produce validated fracture mechanics parameters form different geometries for this purpose. The procedure highlights recommendations for improved test methods so that verifiable material properties are collected. This allows the modelling methods using standard laboratory and feature component data to be used with increased confidence in life estimation codes. This pre-standardisation work is of relevance to ASTM, ISO, ASME, API (American Petroleum Institute) and PVRC (Pressure Vessels Research Council (USA)) as well as to allow further improvements to life assessment CoP such as R5, BS7910 and

A16. Clearly the recommendations resulting from this CoP will be useful for increasing confidence in defect assessment codes. In addition the similarities of the approaches in the various codes do not necessarily imply that calculations by the different methods will give the same predictions. It may be possible that under certain controlled and validated circumstance the predictions can be optimised. It is clear that a critical comparison is only possible when the same method is used on another material and condition or the same test cases are examined by the different codes [11-17].

2 Creep Crack Growth Parameters

Typically, fracture mechanics concepts are used to characterise crack initiation and growth at high temperatures. Usually at short times the stress intensity factor K, or the elastic-plastic parameter J, is employed to describe the stress and strain distributions at a crack tip whereas at long times, when steady state conditions have been reached, the creep fracture mechanics term C^* is most commonly adopted [18-26]. During the intervening stage damage formation and stress redistribution is occurring at the crack tip. The parameters are validated by the correct usage of parameters to describe creep brittle and creep ductile crack growth [8].

2.1 Steady State Creep Crack Growth (CCG) Analysis

Creep crack growth rate under steady state for a creep ductile material is usually analysed using the fracture mechanics parameter C^* [18-26]. The derivation for C^* which is analogous to J is well documented [18] and will not be detailed in this paper. Once a steady-state distribution of stress and creep damage has been developed ahead of a crack tip, it is usually found that creep crack growth rate () can be described by an expression of form ;

$$\dot{a} = D \cdot C^{*\phi} \tag{1}$$

Where creep dominates most often the constants in Eqn. (1) are obtained from tests that are carried out on compact tension (C(T)) specimens

based on the recommendations of ASTM E1457 [8] standard and hence, C^* is estimated experimentally from measurements of creep load-line displacement according to the experimentally determined value of C^* given by

$$C^* = \frac{P\dot{\Delta}^c}{B_n(W-a)} \frac{n}{n+1} \eta \tag{2}$$

where $\dot{\Delta}^c$ is the load line displacement rate due to creep alone, B_n, W and a are the specimen net thickness (accounting for side-grooves), width and crack length, respectively, n is the creep stress exponent. The geometry function η from [18,24] is given as

$$\eta = -\frac{1}{m} \frac{dm}{d\,(a/W)}. \tag{3}$$

Where m is a function of collapse load of the cracked body [24]. Solutions for the η functions, in different geometries, based on analytical solutions (limit load analyses) and finite element calculations are available [24]. From Eqn. (2) therefore providing that the displacement rates can be measured it is possible to simply derive C^* experimentally [25,26] for subsequent use in Eqn. (1).

Stress relaxation of the residual stresses due to creep and crack extension should also be taken into consideration. However no specific allowance is included in standards for dealing with these variations. Where inhomogeneous materials and weldments are involved the above method can be used to derive the appropriate parameter [27]. The method of calculating C^* presented in this paper and adopted by ASTM [8] uses the specimen's creep displacement rate to estimate C^* which inherently takes into account the inhomogeneity in properties by using the instantaneous measured creep strains. Also any variation in the creep strains during the test will reflect both properties change and stress relaxation of residual stresses and will be reflected in the C^* estimation.

2.2 Reference Stress Method for Estimating C^*

The data obtained from C(T) specimens using Eqn. (1) is considered as 'benchmark' material data for creep crack growth properties of the materials in the same way as creep strain rate and

rupture for uniaxial creep tests. These data can be employed directly in crack initiation and growth models described in the different codes [3-7] to estimate residual lives in components. For components such as pipes and plates, on the other hand, C^* must be determined from finite element analysis or reference stress methods. For this the reference stress procedure is adopted in line with that used in the defect assessment codes [3-7]. With this approach C^* is expressed approximately as [18]:

$$C^*_{ref} = \sigma_{ref} \cdot \dot{\varepsilon}_{ref} \cdot \left(\frac{K}{\sigma_{ref}}\right)^2 \tag{4}$$

where $\dot{\varepsilon}_{ref}$ is the creep strain rate at the appropriate σ_{ref} for the component and K is the stress intensity factor corresponding to the applied loading. When the creep strain rate $\dot{\varepsilon}$ at an applied stress σ can be described in terms of the Norton creep law [18]:

$$\dot{\varepsilon} = A \cdot \sigma^n \tag{5}$$

where A and n are material constants at constant temperature. Thus, Eqn. (4) can be rewritten as:

$$C^*_{ref} = A \cdot \sigma_{ref}^{n-1} \cdot K^2 \tag{6}$$

The typical value for n is between 5 and 12 for most metals. In addition, the concept of the average creep rate, $\dot{\varepsilon}_{Ave}$, obtained directly from rupture data, has been used to account for all three stages of creep as an approximate method for estimating the average creep rate $\dot{\varepsilon}_{Ave}$ as shown and defined by

$$\dot{\varepsilon}_{Ave} = \frac{\varepsilon_f}{t_R} = \dot{\varepsilon}_o \cdot \left(\frac{\sigma}{\sigma_0}\right)^{n_{Ave}} = A_{Ave} \cdot \sigma^{n_{Ave}} \tag{7}$$

where σ is the applied stress, ε_f is the uniaxial failure strain, t_R is the time-to-rupture and A_{Ave}, n_{Ave}, σ_o and $\dot{\varepsilon}_o$ are material constants.

2.3 Crack Initiation (CCI) Analysis

When a structure containing a defect is first loaded the stress distribution is given by the elastic K-field or the elastic-plastic J-field. Therefore, time is required for the stresses to redistribute to the steady-state creep stress distribution

controlled by C^*. During this period, transient conditions exist which are not uniquely defined by C^*. In addition, a period of time is needed for creep damage to develop around the crack tip. Furthermore due to the practical limitations of crack detection equipment, the initiation of crack growth is difficult to determine precisely. Typically, this ranges between an extension Δa of between about 0.1 and 0.5mm depending on component and crack dimensions. For laboratory specimen such as CT, ASTM E1457 [8] identifies an extension of 0.2mm to cover the entire transition time to steady state conditions and this distance also takes into account the resolution of crack monitoring equipment. However, in order to increase the confidence in the crack measurement of the different components, it has been determined, in this present work, that $\Delta a = 0.5$mm was the best value to choose to compare both the CT data and the semi-elliptical defects in the pipes and plates.

From Eqn. (1) it may be expected that the time, t_i, to initiate a crack extension of Δa can be expressed by:

$$t_i = D_i \cdot C*^{\phi_i} \tag{8}$$

where D_i and ϕ_i are material constants. For steady-state cracking D_i is expected to be given approximately by $\Delta a/D$ with $\phi_i = -\phi$ and hence Eqn. (8) can be re-written as follows [25,26]:

$$t_i = \frac{\Delta a}{D} \cdot C*^{-\phi_i} \tag{9}$$

This equation assumes that the entire initiation period is governed by steady-state C^*. This cannot be expected to be true during at least part of the initiation period t_i. The applicability of the equation has been examined for the pipes and plates [9] in the same as has been done for crack growth.

2.4 Fatigue Crack Growth (FCG) Rates

For fatigue crack growth it is assumed that the mechanism is time and temperature independent and K or J dominates at the crack tip. At room temperature under cyclic loading conditions, crack propagation usually occurs by a fatigue mechanism where the Paris Law can describe crack growth/cycle $(da/dN)_f$ in terms of

stress intensity factor range ΔK by

$$(da/dN)_f = C' \Delta K^{m'} \tag{10}$$

Where da/dN is fatigue crack growth rate per cycle, C' and m' are material dependent parameters, which may be sensitive to the minimum to maximum load ratio R of the cycle. The procedure for fatigue crack growth testing is well known [28]. However for low frequency dwell periods where creep dominates the parameter of choice would be the same as for static creep testing such as C^* [18,29].

2.5 Analysis of Creep/Fatigue Crack Growth (CFCG) Rates

At elevated temperatures combined creep and fatigue crack growth may take place. However in most cases fatigue dominates at higher frequencies ($f > 1$Hz) and creep dominates at lower frequencies and dwell periods ($f < 0.1$Hz) [29]. In most cases the total crack growth crack growth calculations under cyclic loading can be described as

$$(da/dN) = (da/dN)_c + (da/dN)_f \tag{11}$$

Where this linear summation combines creep and fatigue components. This can be refined using the method given in the British Energy's R5 Procedure [4].

Total crack growth per cycle, (da/dN), can be described by Eqns. (1), (10). It can be shown that a simple cumulative damage law can be applied to describe creep/fatigue interactions [29]. Fatigue analysis is usually conducted by using the linear elastic K parameter [9] and the creep portion can be described by C^* [29].

3 Geometries Used in Crack Growth Tests

Originally the Compact Tension C(T) specimen was chosen as the recommended geometry for crack growth tests [8]. More recent work has validated a wider range of geometies [13,25]. The VAMAS procedure, therefore, recommends a wider range of geometries for testing at high temperatures [9]. The geometries can be placed in two categories. The first are the recommended

standard fracture mechanics specimens and the second are the 'feature specimens' which cover all non-standard test specimens which could resemble components. These categories are described in detail in the draft VAMAS ISO/TTA document [9]. The laboratory specimens used to derive CCG and CCI properties [13,14, 25] consist of <u>C</u>ompact <u>T</u>ension (C(T)), <u>C</u>-<u>S</u>haped <u>T</u>ension (CS(T)), <u>S</u>ingle <u>E</u>dge <u>N</u>otched <u>T</u>ension geometry, (SEN(T)), <u>S</u>ingle <u>E</u>dged <u>N</u>otched <u>B</u>ending geometry, (SEN(B)), <u>D</u>ouble <u>E</u>dge Notched <u>T</u>ension geometry, (DEN(T)), <u>M</u>iddle <u>T</u>ension or <u>C</u>entre (through) <u>C</u>racked Panel in <u>T</u>ension, (M(T) or CC(T)). Example results for these specimen types are shown below.

3.1 Fracture Mechanics Specimens

As a result of EU collaborative programmes [10-16] especially in HIDA [11], LICON [12] and CRETE [13] tests and analysis were performed on a number of fracture mechanics geometries. The VAMAS procedure [9] uses the information provided by these programmes to analyse data for the above six geometries, that have now been verified for the purpose of creep and creep/fatigue crack growth and initiation testing and by comparing the results to C(T) test data [25]. These will now be implemented in the next update of ASTM 1457 standard for creep crack growth. The listing of specimens does not mean that other geometries should not be used for testing but that they would need validation before their inclusion in the procedure. Detailed dimensions, machining instructions methods of setting up and limits of testing accuracies are described in the procedure.

An example of CCG data from the different specimen types are shown in Figure 1. Figure 1a shows the normalised crack growth versus time for the different geometries. The range of scatter in the raw data is usual for CCG. Figure 1b shows the correlation of the data with C^* when compared to the C(T) databand of the same 316H type stainless steel material [19]. This suggests that for the range of sizes and geometries used the crack growth data obtained is comparable to within the inherent scatter of data. The details attached to verifying crack growth properties data in

standards [25-9] is an indication of its importance to improving life assessment results.

The specimens discussed above relate to parent and homogenous test specimens. There are no recommendations or procedures in codes at present to extend the experimental method to weldments and inhomogeneous material even though these have been extensively tested [11-12, 27].

The main objective for testing weldments is to consider regions in components where welds are likely to fail and derive data for them. Figure 2 shows a schematic example of how to locate the region of interest in a specimen. The Heat Affected Zone region (HAZ), in this case, is placed in the line of the crack path in order that it may crack and produce crack growth properties for that region. This is an ideal representation and in many cases the cracking follows a path of least resistance and may therefore deviate from the required path. It is also important to identify the material properties surrounding the region of interest as they will contribute to the behaviour of cracking in the region. This line of research is continuing in order to quantify the relevant parameters [9].

In characterizing crack growth data of HAZ C(T) tests an example is presented in Figure 3a showing the CCG versus time for various weld specimens of 316H at 550°C. A clear difference between the CCG in the parent (Figure 1a) and CCG in the HAZ (Figure 3a) is the way cracking tends to take longer to initiate and then fails more abruptly. Figure 3b shows the correlation of the same data with C^* as discussed above following the ASTM procedure [1,8,27]. It is seen in Figure 3b which uses Eqn (2) to derive C^*, that the crack growth data from all specimens tend to fall within the same scatter band. Also shown in Figure 3b (indicated as C(T) PM) is the data band for tests performed on a range of C(T) specimen sizes (W = 100, 50 and 25 mm) for homogeneous parent material, taken from [25]. It may be seen that the measured CCG rate in the HAZ is substantially higher than that in the homogeneous parent material (PM) specimens and the extent of data scatter for the weldment is comparable to that of the par-
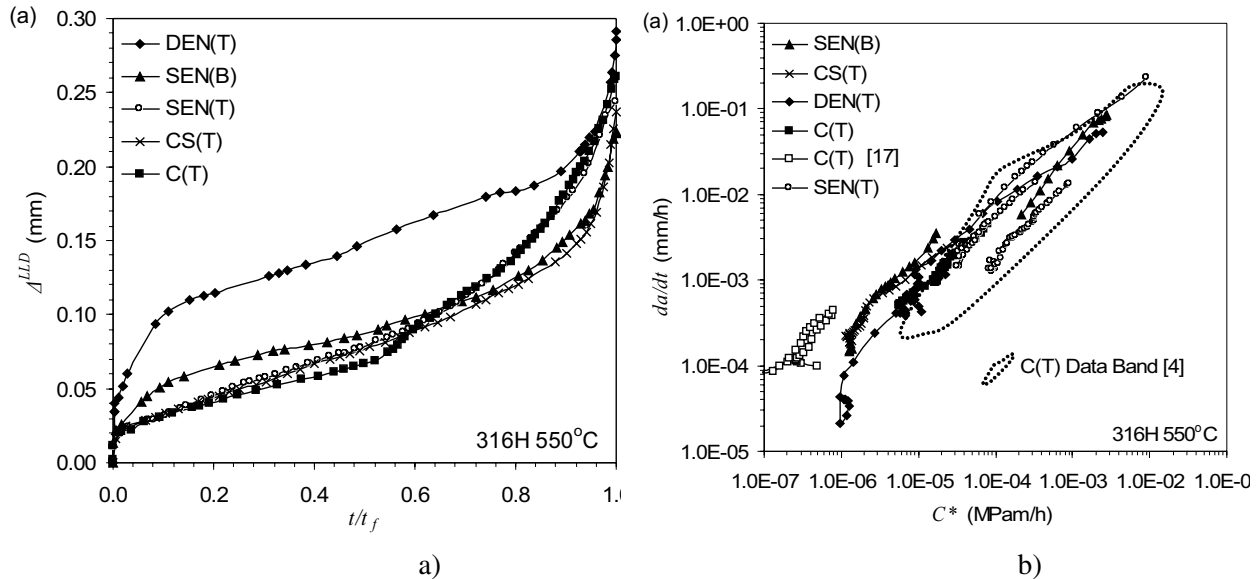
a)   b)

Figure 1: a)Example of normalised crack length versus time data and b) Comparison of the creep crack growth rates with C^* for different geometries with the C(T) databand [19], for $\Delta a \geq 0.2$mm, in 316H stainless steel at 550˚C. [19,25]
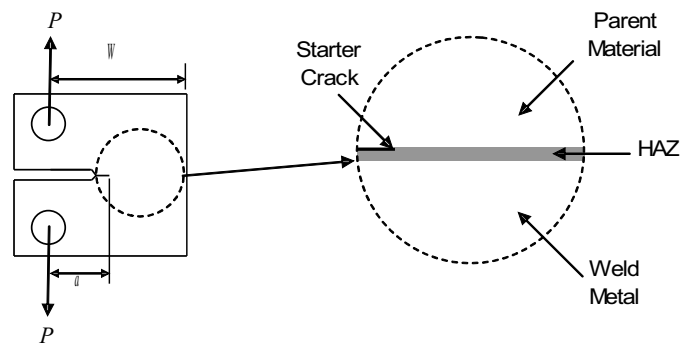

Figure 2: Schematic of C(T) specimen indicating the position of the starter crack and of the weld, HAZ and parent material regions.

ent material specimens.

The advantage of using this type of validated data as material properties data for life assessment is that a direct comparison can be made with the behaviour of different alloy conditions. Also depending on the level of safety required the mean or the upper-bound of the relationships can be utilised to increase conservatism in remaining life predictions.

3.2 Feature Specimens

A step towards a component shape is the use of feature type specimens, which can represent

different component geometries. These have also been tested for verification and validation in different collaborative programmes [9-11]. A schematic of these types of specimens are shown in Figure 4. These consist of pipes, plates and solid notched bar cracked specimens. The testing of such specimens is costly and difficult and is not recommended as a routine procedure for deriving data but they can be used to validate the laboratory data in comparison to components [9].

Analysis of component or feature component testing was an important part of VAMAS TWA25 procedure [9]. It has been shown previously that although different codes employ Eqns. (5-7), of-
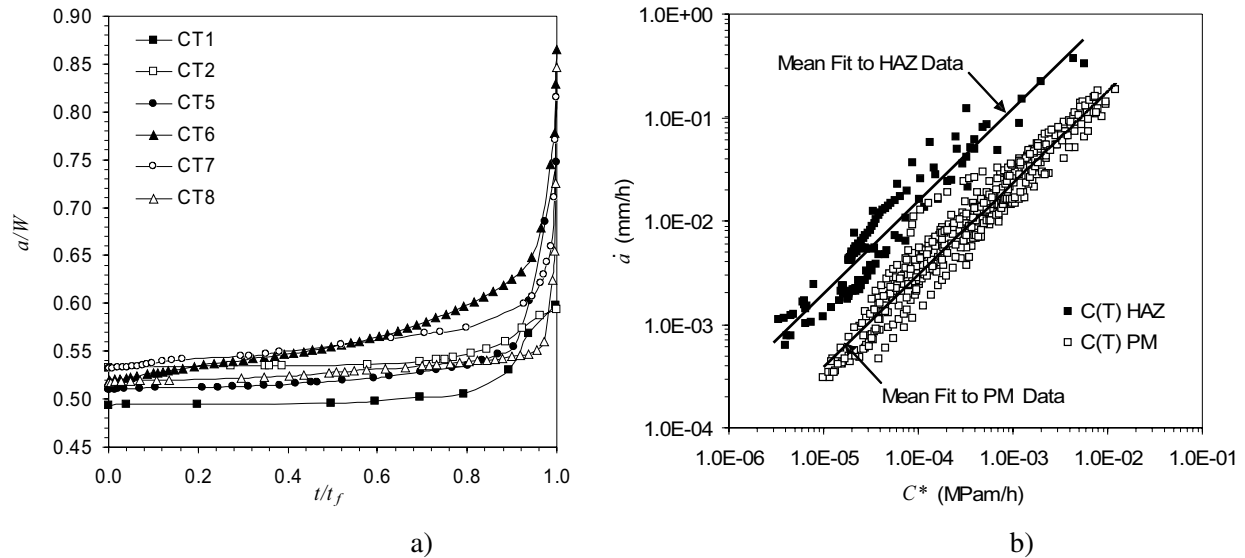
a)   b)

Figure 3: a) Normalised crack length with normalised time for HAZ 316H C(T) tests b) Comparison of the mean fit to the creep crack growth rates with C^* for HAZ and parent material (PM) C(T) specimens tests at 550°C [27]
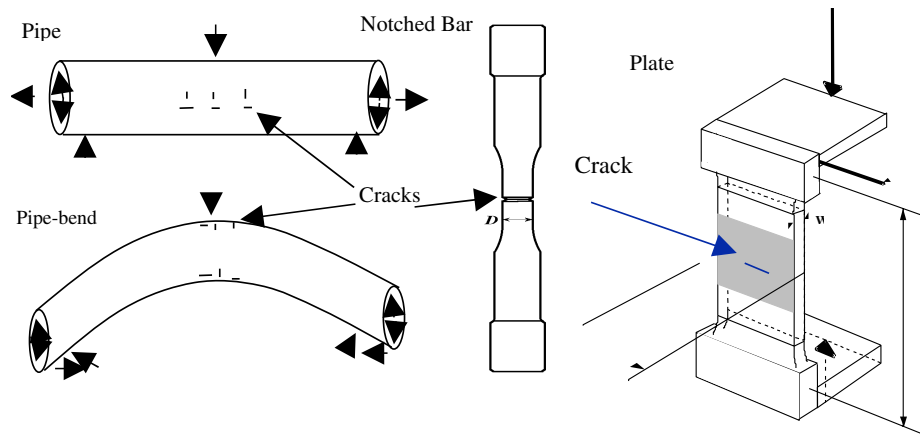

Figure 4: Feature geometries showing a pipe, pipe-bend notched bar with circumferential crack and plate under bending and tension feature specimens showing crack and loading positions [9].

ten different formulae are used to evaluate K and σ_{ref}. Greater sensitivity of C^* and cracking rate to reference stress than to K is expected from Eqn. (5) since ϕ in Eqn. (1) is close to one, and typically $n \gg 1$ and evidence of this has been demonstrated previously [30]. It has also been previously demonstrated that 'global' collapse solution represent best correlation of the cracking behaviour in pipe and plate components [9].

Furthermore since it has been shown [30] that there is no absolute correct solution for reference stress in components and that in order to get an overall agreed definition compromises have to be made. This would mean that the codes adopt a standard formula for the derivation. It may be possible by using detailed FE analysis of the geometry in 3D and the right boundary conditions and material properties to improve the solutions in the future. But for the present it is more important to be able to compare inter-laboratory data and reach definitive comparison with the results. Hence the recommendations in the CoP [9] of specific formulae for evaluating the C^* parameter is of importance since this will reduce the uncer-

tainty when data are compared between different laboratories. Some examples of the comparisons of data for the plate and pipe with C(T) specimens are given in the next section to highlight the analysis and the difficulties that exist in producing and treating the data from feature test.

3.3 Geometry Definitions for Plate Components

For plates there exist several reference stress solutions [3-7] which use Eqns. (4),(6) to derive C^*. However in the VAMAS procedure [9] one reference stress solution is recommended. It has been shown that for small partially penetrating defects in plates subjected to combined tension and bending loading, these reference stresses can significantly over-estimate creep crack growth rates. Therefore a recommended reference stress, which is based on a global collapse mechanism, is expressed as follows:

$$\sigma_{ref\ Plate} = \left\{ (\sigma_b + 3 \cdot \gamma \cdot \sigma_m) + \left\{ (\sigma_b + 3 \cdot \gamma \cdot \sigma_m) \right.\right.$$
$$\left. + 9 \cdot \sigma_m^2 \cdot \left[(1-\gamma)^2 + 2 \cdot \gamma \cdot (\alpha - \gamma) \right] \right\}^{1/2} \right\}$$
$$\left/ \left\{ 3 \cdot \left\{ (1-\gamma)^2 + 2 \cdot \gamma \cdot (\alpha - \gamma) \right\} \right\} \right. \quad (12)$$

where $\gamma = (a \cdot c)/(W \cdot l)$ and $\alpha = a/W$. In these equations, a is crack depth, c is half crack length at the surface, W is the thickness of the plate and l is the half-width of the plate, respectively.

Figure 5 gives and example of comparing the effects of frequency and the plate geometry for a 316LN type stainless steel tested at 650°C [11,30]. Figure 5a shows that for low frequencies the crack growth data for this steels lies within the scatter of the static load data, suggesting that the cracking is time dependent and due to creep at low frequencies. It should also be noted that there increased scatter in the data form feature tests. Figure 5b compares the same databand with data from plate tests. In this case there is a clear difference between negative R ratios and the rest of the cyclic test data of the plate lying at the upper and lower bounds of the C(T) databand respectively. This suggests that caution would be needed in using standard laboratory tests to predict component

behaviour where negative R-ratios are present. It is also clear form such comparisons that a comprehensive validation of different materials, geometries and loading conditions should be performed to validate the procedures fully.

3.4 Geometry Definitions for Pipe Components

In the same way as the plates Eqns. (4),(6) are used to derive C^* for pipe geometries. Equations For a range of pipes also exist to derive K and reference stress. It has been shown that solutions for K due to Raju and Newman [31] and the 'global' collapse solution for the reference stress are best to estimate C^* in the analysis for pipes. 'Global' solutions of reference stress are based on the collapse of the entire cross-section at the site of a defect. For a semi-elliptical axial defect in a pipe subjected to an internal pressure p, R6 [5] gives the reference stress as:

$$\sigma_{ref\ Pipe} = \frac{p}{\frac{1}{R_e - a} \cdot bate\,(a,c) + \ln\left(\frac{R_e - a}{R_i}\right)} \quad (13)$$

where $bate(a,c)$ is given by :

$$bate(a,c) = \frac{a}{\sqrt{1 + 1.61 \cdot \frac{c^2}{[(R_e - a) \cdot a]}}} \quad (14)$$

where $bate(a,c)$ function of dimensions, a is crack depth, c is half crack length at the surface and R_i and R_e are the internal and external radii of the pipe, respectively.

Figure 6a gives an example of comparison of crack growth analysis of the C(T) and pipes geometries in both parent and weld P22 steel tested at 565°C. Figure 6a shows little difference between parent and heat affected zone (HAZ) region tests for the C(T) P22 specimen which is contract to the 316H HAZ behaviour shown in Figure 3. On the other hand Figure 6b, for the pipe test whilst not showing a noticeable difference between parent and HAZ cracking does show an effect due to geometry when compared with the databand of Figure 6a. This could be due to either differences in constraint, or that the cracking in the pipe has not reached steady state as well as the fact that derivation of CCG from pipe tests are

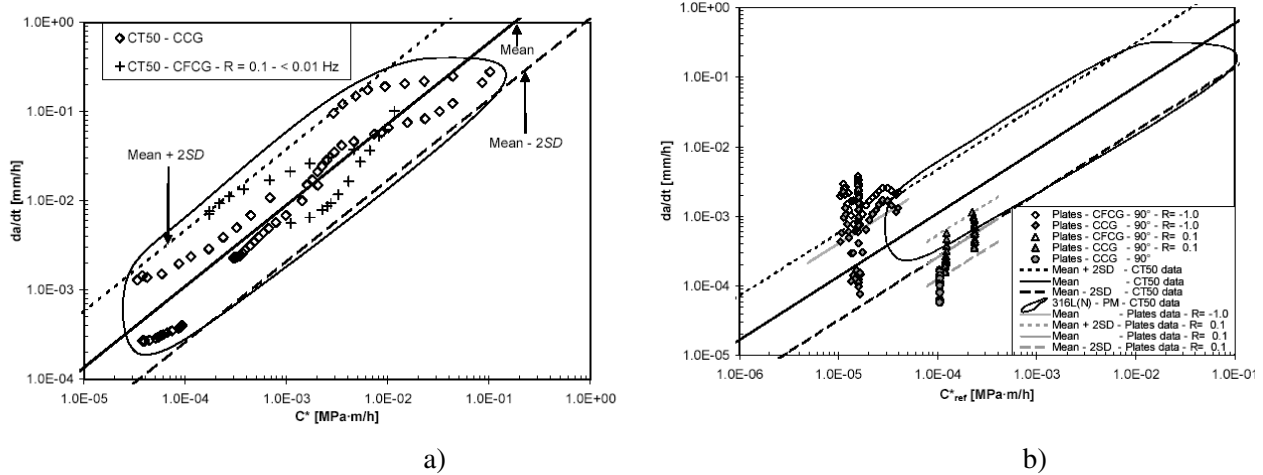a)   b)

Figure 5: Effect of static and cyclic loading on crack growth rate, for 316LN at 650°C for a) C(T) specimens [11] showing the range of data scatter and b) comparison of plate crack growth data at different frequencies with the same C(T) databand as in Figure 5(a) [30]
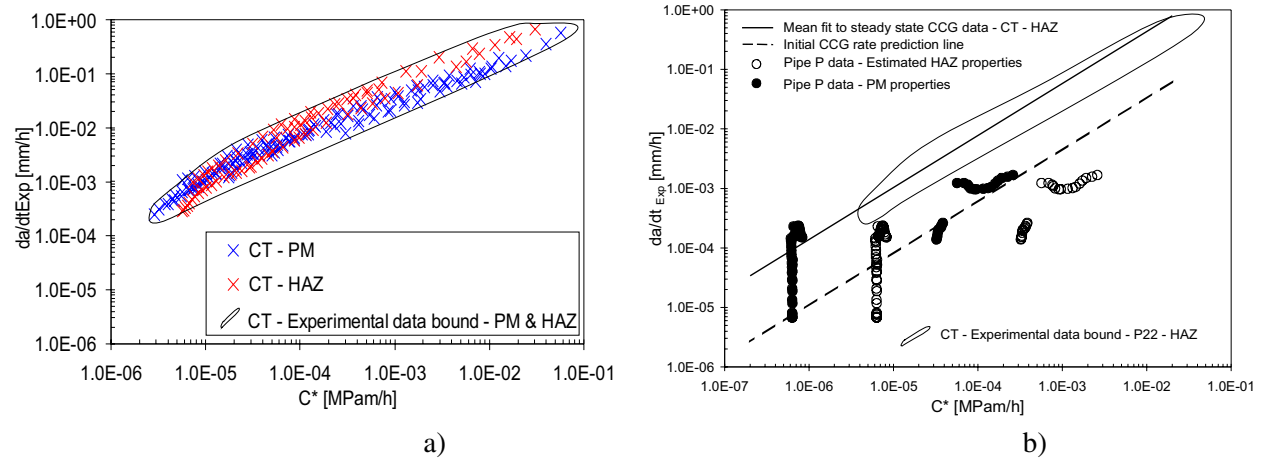

a)   b)

Figure 6: a) Comparison of welded and parent crack growth rate for P22 steel tested at 565°C, and b) Comparison of crack growth versus C^* for P22 C(T) and pipe specimens with C(T) data band (Figure 6a) showing the effects of geometry on crack growth [11].

much more difficult than for standard C(T) specimens [30]. All these factors highlight the importance of more tests to improve the validation of laboratory data with component data.

4   Treatment of Residual Stress

Residual stresses can arise from welding and fabrication. If a tensile residual stress remains in the component there is a clear likelihood that CCG will be affected. Therefore the effects of residual stresses on component life need to be accounted for within the life assessment procedures. If the

operating temperature of the component is in the creep regime, the redistribution effects help relax the crack tip stresses but at the same time local damage due to pre-strain could help enhance cracking. The effects of the residual stresses can be taken into account in the calculations of the fracture mechanics parameters K and C^* but the effects of material damage on CCG and CCI will need further consideration. It is important that such stresses are considered in safety assessment procedures such as the UK structural integrity procedures, R6[1] and BS7910[2].

4.1   *Residual Stress Profiling*

Since information on residual stress distributions is often not directly available, compendia with recommended (upper-bound) residual stress profiles for use in an integrity assessment are included in R6 and BS7910. However the effects due to re-distribution are not considered in a quantitative manner at present in these codes. In order to highlight these effects a comprehensive residual stress profile is needed [32-34]. This was derived from a range of steels and different geometries that have been welded, cold bent, repair welded or overloaded. Stress profiles were collated from data available in the public domain for various types of weld geometries were also examined in this study. The measured data covers a range of conditions such as materials, measurement methods, plate thicknesses, weld heat input and boundary restraints. The materials included in the present geometries are ferritic, austenitic, C-Mn and Cr-Mo steels. The measurement methods used include neutron diffraction, X-ray diffraction, hole-drilling and sectioning, block removal, trepanning, slotting and hole drilling [33]

The residual stress profiles for T-plate and tubular T-joint in the assessment procedures of R6 and BS7910 are shown in Figure 7a. These profiles have invariably been chosen from upperbouns of available case specific datasets. Figure 7b shows the results of the statistical bests fits of the proposed new profile [33] which within the data scatter encountered, is material, geometry and condition independent. The proposed method considers simple profiles based on the mean and membrane shifts across the thickness of the geometry. Figure 7b presents three profiles that can be used. It is also assumed that any compressive stresses are taken to be zero across the net section. When all profiles are compared with that of the present statistical curve it can be seen that depending on which line is chosen in Figure 7b the profile could be more or less conservative than the case-specific profile in Figure 7a. This will be discussed in the next section when these profiles are used to estimate the stress intensity factor K which are used in Eqns. 5 and 10 to derive C^* and K used in the analysis of CCG and CFCG data.

Furthermore the likelihood of over-conservatism of such profiles exists when used at high temperatures. The profiling of redistributed residual stresses has not been considered properly in codes. Recent work suggests that there is a rapid reduction of residual stresses within a short time at temperature [34-37]. As an example a redistribution analysis of the residual stresses by modelling a plastic overload was carried out in a T-Plate using a kinematic hardening model and the Norton's creep law [34]. In this analysis the power-law Norton's creep equation was used. A sensitivity analysis for the creep properties for the type 316H stainless steel was carried out for the T-plate using the 4PB model and the cantilever beam model. The redistribution analysis was carried out for the cases of plane strain (PE) and plane stress (PS). The hold time at the temperature of 550˚C was upto 10 000 hours (1.14 years). Using Figure 7b as the comparison of distribution profiles at time=0hours, Figure 8 shows the redistribution profiles derived from the creep relaxation modelling analysis [34]. It is clear that there is a rapid drop in stresses at the surface of the specimen, due to redistribution, in the first 1000H using any of the fits. These results need to be further verified by experimental relaxation tests of the components followed by residual stress measurements. However this establishes the fact that the present residual stress profiles used for low temperature characterization is likely to be over conservative. It should also be noted that damage an reheat cracking is also likely to occur at the early stages before relaxation takes effects as shown. These aspects will be discussed in section 5.

4.2   *Estimating Stress Intensity Factor (SIF)*

Using Residual Stress Profiles

Since information on residual is available as profiles across the thickness of geometries it is possible to make estimates of the stress intensity factor (SIF) K for different geometries. Using Figures 7 and 8 and applying a weight function to derive the effective K for a four point bend geometry. A direct comparison of the level of conservatism can

(a) Distribution profile in R6 and BS7910

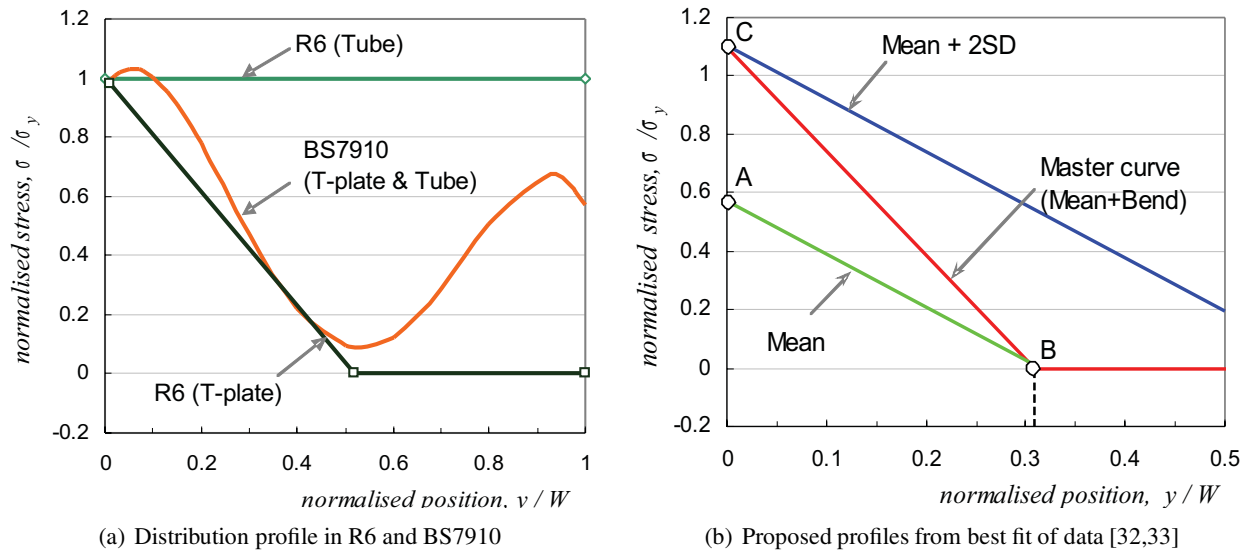(b) Proposed profiles from best fit of data [32,33]

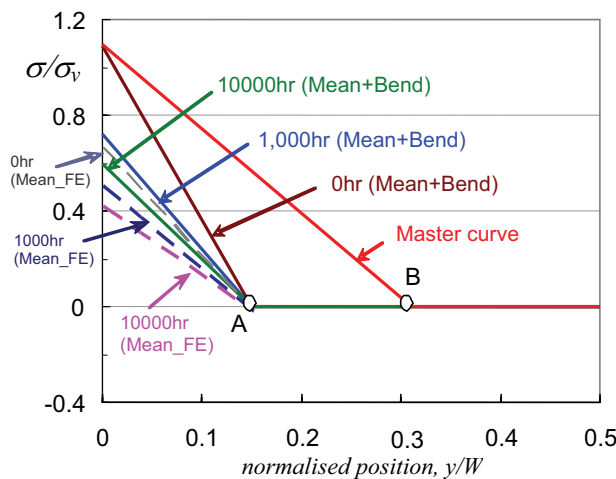Figure 7: Suggested residual stress distribution profiles for T-plate and tubular T-joint

Figure 8: Comparison of experimental 'Master curve', and 'Mean+Bend' and 'mean' profiles with predicted stress redistributions of 316H steel at 0, 1000 and 10,000 hold-time at 550°C [34].

be made between the various profiles both initial and redistributed [32-34]. Figure 9 compares, for two geometries, the SIF results from the profiles to those from measured residual stresses derived for a S355 steel [34]. The normalised SIF values obtained using the recommended distributions of R6, BS7910, and 'Master curve' are shown in Figure 9a for the T-plate and in Figure 9b for the tubular T-joint.

For the T-plate, the BS7910 distribution is the most conservative, and the 'Master curve' gives less conservative SIF than BS7910 and R6 as

shown in Fig. 5(a) when comparing with the SIF due to the measured distributions. For the tubular T-joint, 'Master curve' again gives less conservative SIFs than R6 and BS7910 as shown in Fig. 5(b). From these results, that although the 'Master curve' is a simplified profile for residual stresses it is still less conservative than existing distributions of R6 and BS7910.

Consideration of residual stresses relaxation at high temperature further establishes the fact that the present profiles should take into account these effects. Figure 10 shows the plot of the effec-
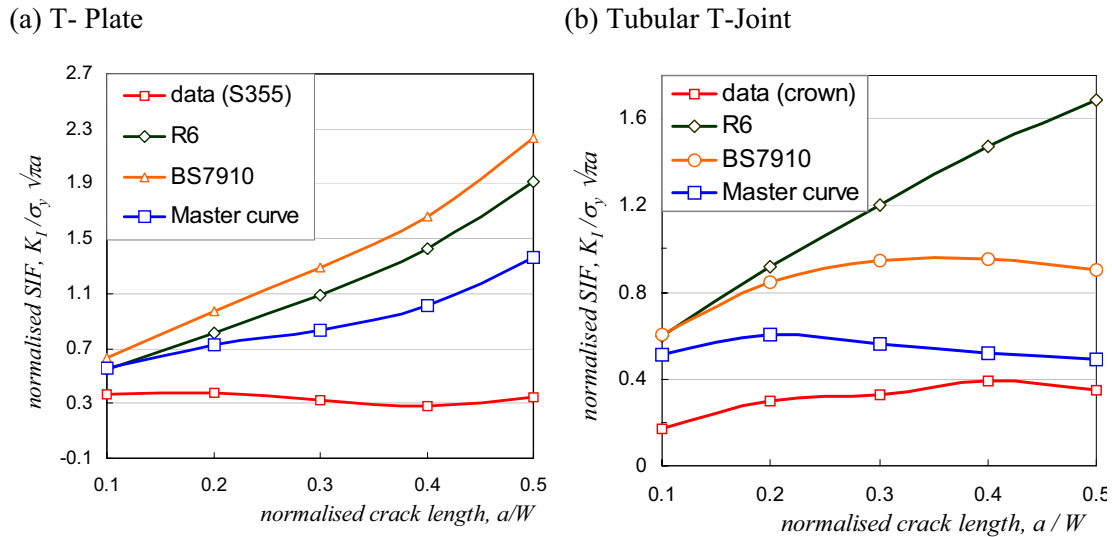
(a) T- Plate

(b) Tubular T-Joint

Figure 9: Stress intensity factors derived from residual stress profiles in Figs. 7 [34]

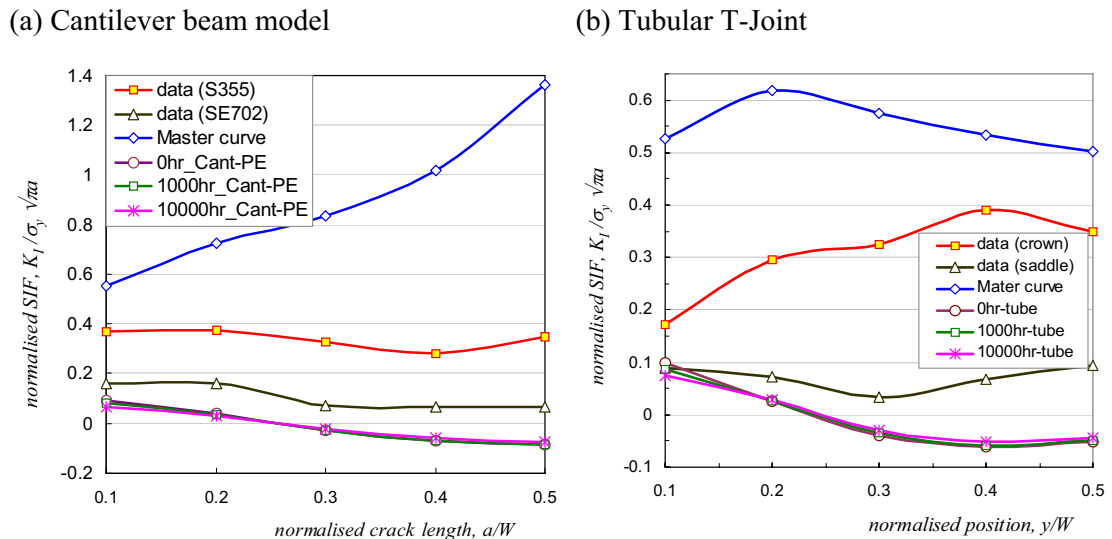(a) Cantilever beam model

(b) Tubular T-Joint

Figure 10: Comparing effective K using predicted residual stresses in a Cantilever Beam model and a Tubular T-joint in two steels [34] with the calculated effective K using the upper bound 'master curve' and the redistributed curves in Fig. 8.

tive SIF across the thickness for a 4-point bend beam model [34]. As redistribution data was not available only experimental measurements of un-relaxed residual stresses in two steels are compared. It is clear that the various profiles could produce wide range of predictions and that if residual stress redistribution were taken into account the estimated SIF values would substantially decrease.

5 Modelling Induced Residual Stresses

Any assessment procedure needs relevant data and models in order to estimate remaining life from available information. Where residual stresses might exist a measure of structural response over time during which creep and fracture occurs is needed. Following welding or fabrication there are invariably residual stresses induced in the interface region. These cannot be mea-

sured on an individual basis and validated numerical simulation can be used to obtain residual stress profiles. One way to model residual stresses in a controlled manner are to induce residual stress in a using a plastic over-load in a geometry containing a sharp or blunt crack [36-38]. In this way both numerical and residual stress measurements can be calculated and compared in an experiment. The finding will assist in the understanding of the effects of residual stresses and the subsequent relaxation on creep crack growth.

5.1   Mechanically Induced Residual Stress

The effect of mechanically induced residual stress on creep deformation and fracture in C(T) specimens containing notches and sharp cracks is presented to show an example of the experimental and numerical methods involved in quantifying the behaviour. The C(T) specimen, illustrated in Figure 11, has been used [35,36] in the form shown. Figure 11shows schematically how the overload is inserted and the regions in which plastic damage occurs at the crack tip. Figure 11b shows where the residual stress measurements are taken following plastic overload and subsequent stress relaxation at temperature. In addition to the experimental program, the plastic overload and the subsequent creep response was modelled using FE analysis to predict the stresses, strains and creep damage [35-38].

In order to enhance the effect of residual stress, a creep brittle Type 347 austenitic steel manufactured from numerous runs of manual metal arc (MMA) welding was examined [36-38]. The example presented was modelled to compare measured and predicted residual stress generation and relaxation at 650°C for this steel.

5.2   Pre-Compression of C(T) 347 Weld Specimens

A schematic of the notched specimen is illustrated in Figure 1a in which some of the key parameters are indicated as the applied compressive load is P; Δ is the load point displacement, Δ_m the notch opening; r_p is the size of the plastic zone directly ahead of the notch root after unloading. FE analysis was carried out to identify an appropriate

load for pre-compression to result in a sufficiently large tensile residual stress ahead of the notch. The compression was carried out at room temperature where the majority of the inelastic deformation is rate independent; subsequently the specimens were tested under constant load at 650°C where rate dependent (creep) effects dominate. In the pre-compression analysis both isotropic and kinematic hardening was examined [36-38].

5.3   Redistribution and Damage Accumulation at High Temperatures

The stress relaxation was modelled and the material model used was the RCCMR primary and secondary creep model [2], with material parameters appropriate to Type 347 weld. Figure 12 illustrates the predicted stress relaxation in the element which has the largest initial residual stress (a distance of approx. 2.3mm from the notch root). The predicted residual stress field directly ahead of the notch from the 3D finite element analysis is shown in Figure 13b [37]. In Figure 13b stresses are normalised by the room temperature 0.2% flow strength ($\sigma_{0.2}$ = 480MPa). It is seen that after 10 hours almost 40% of the stress has redistributed and after 10,000 hours the peak stress has relaxed to approx. $0.25\sigma_{0.2}$.

The measured residual stress, following pre-compression and after 1000 hours at 650 °C, is shown in Figure 13a. A significant reduction in stress in the local region of the notch tip is noted. it is seen that although the average stress levels predicted by the models are close to the measured values, creep models (calibrated using uniaxial data from either relaxation or creep tests) fail to predict the significant stress relaxation close to the notch. This lack of agreement between FE and measured stresses following high temperature exposure is associated with damage development and cracking in the specimen.

Generally it has been seen that the FE results are in good agreement with the measured stress distribution, though the peak stress is overestimated. The neutron diffraction measurements shown here have been carried out at the ISIS ENGIN-X facility (CCLRC Rutherford Appleton Laboratory, Oxford, UK). Repeat measurements
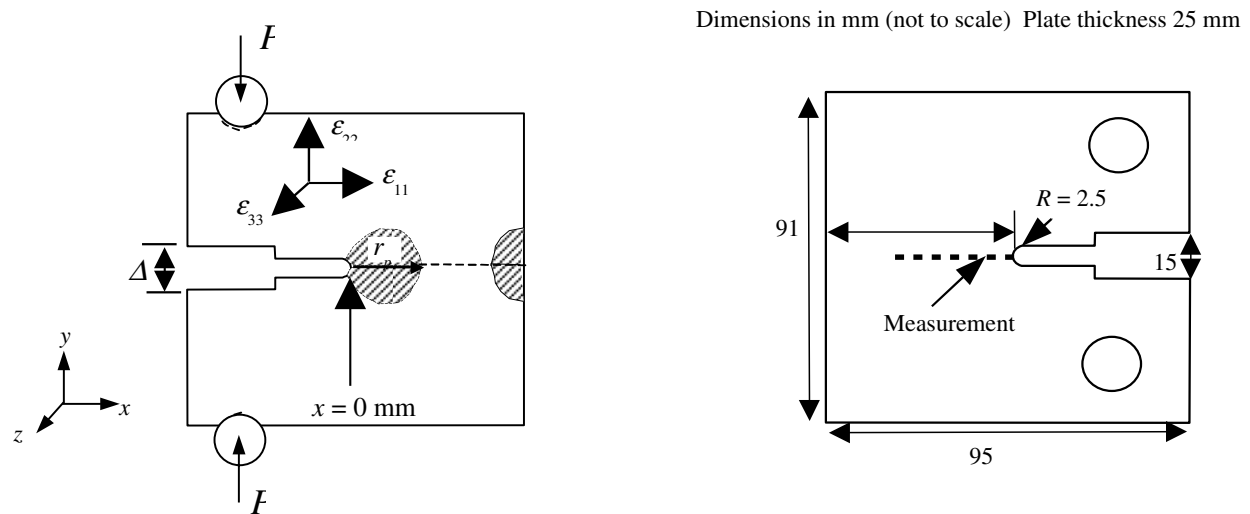
Dimensions in mm (not to scale) Plate thickness 25 mm

Figure 11: (a) Method of insertion of residual stress field and region of residual stress measurement, *P* =applied load, Δ = load line displacement, r_p = size of plastic zone; (b) Specimen dimensions and location of residual stress measurement
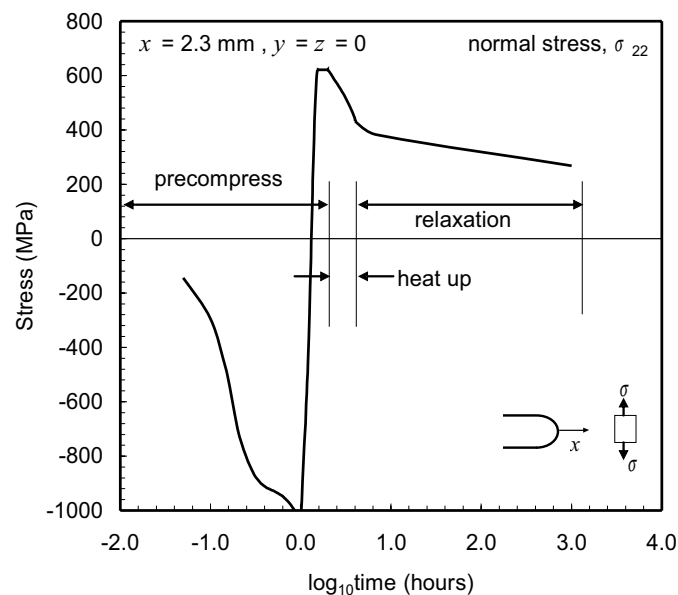

Figure 12: Evolution of notch stress in the specimen.

have also been carried out at SALSA (Institut Laue-Langevin, Grenoble, France) and STRESS-SPEC (FRM-II, Munich, Germany) confirming these results.

In the experiment the C(T) was held at 650°C for 1000 hours. With a purely secondary stress due to the pre-compression it was observed that multiple cracking has initiated as shown in Figure 14. As shown in Figure 15a Experimental observa-

tion of the specimen following 1000 hrs relaxation at 650°C shows that the average measured crack growth was about 4mm from the notch during stress relaxation. This corresponds with the numerical prediction region of tensile stresses shown in Figure 15b [37]. It is noted that the initially high CCG rate decreases with time in a stepwise manner. The form of the graph in Figure 15a is consistent with the observed slowdown in creep
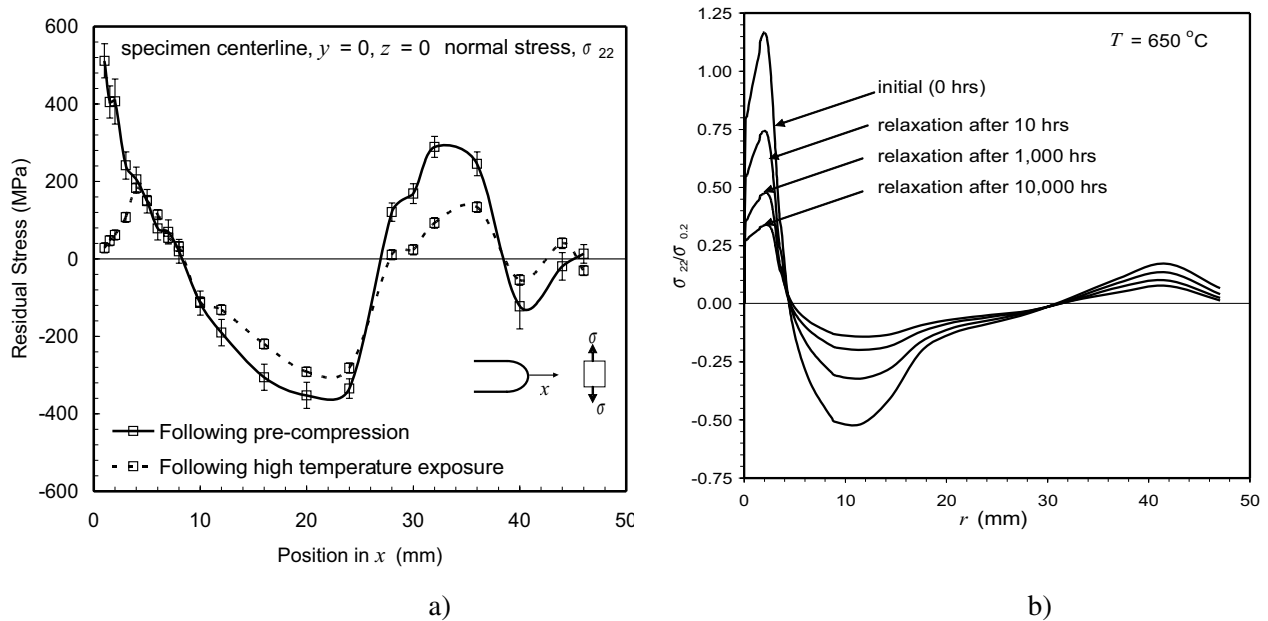
Figure 13: (a) Measured residual stress after pre-compression and after 1000 hrs at 650˚C (b) Predicted normalised stress relaxation at 650˚C for the C(T) 347 weld steel following pre-compression at room temperature [37]
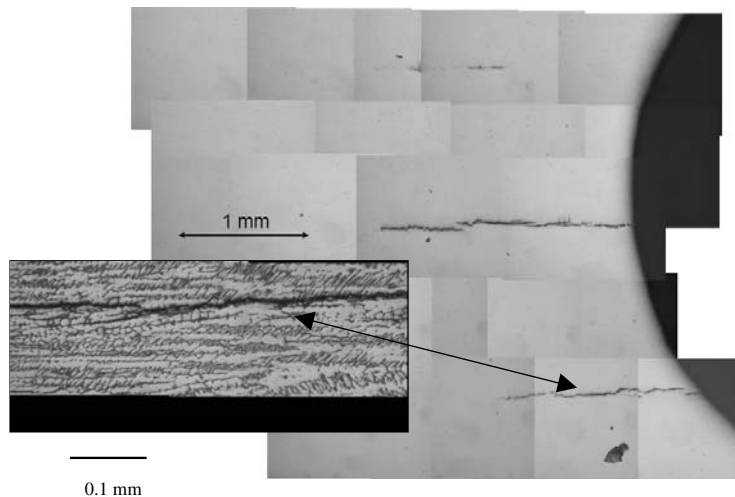

Figure 14: Un-etched and etched region (inset) in the vicinity of the notch in BN6 following 1000 hrs at 650˚C showing multiple cracking and crack in the dendritic region of the weld.

strains and the possibility that the cracking slows down due to both relaxation of stresses as well as entering into the compressive residual stress zone.

These findings suggest that although stress relaxation occurs quite rapidly creep brittle cracking develops and grows within that time period. However the resistance to cracking is attributed to the growth of cracking through the tensile field into the compressive field (see Figure 15a). It is unclear at present if the plastically deformed regions both in the tensile and compression regions of the C(T) plays an additional part in accelerating creep cracking. Future work will need to consider this and also examine whether the rate of crack growth during stress relaxation can be characterised using a single parameter such as C^*.

a)   b)
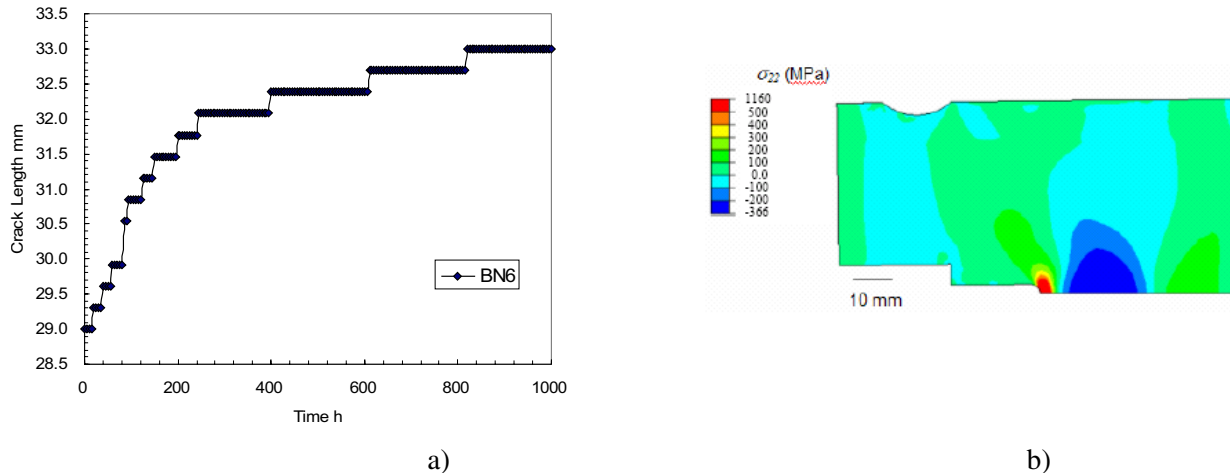
Figure 15: (a) Crack extension for weld 347 specimen after relaxation for 1000h at 650°C, (b) Stress contours showing the tensile and compressive regions at the crack tip after aapplying a compressive load to the specimen (using a displacement ($\Delta = 2$ mm))at load-point [37]

6   Conclusions

Creep and fatigue crack growth models as well as residual defect assessment codes need reliable and verifiable material properties data and validated fracture mechanics parameters for use in their predictive methodologies. Previously codes have incorporated the results for homogenous materials from research results in a number of EU collaborative projects [10-15] to develop an overall methodology for deriving acceptable data and validated parameters for life assessment analysis. The results are also compatible with ASTM E1457 [1] standard for testing C(T) specimens. The fracture mechanics parameter validated for the analysis is the second criteria for improved assessment and life prediction. It is clear that a unified method of deriving reference stresses and the parameter $C*$needs to be adopted to improve inter-laboratory comparison of the data. Therefore the fundamentals employed in the non-linear analysis of reference stress need to be agreed to and solution verified by component tests.

Weldments are an additional complication because of their material inhomogeneity, the possibility of containing micro cracks, residual stresses and their effect on constraint due to their position in the parent structure. Improved understandings of welded structures are therefore crucial to better lifing methods. Residual stresses are seen to be

as an important variable in improving life prediction of cracked components. The capability to produce generic residual stress profiles and their subsequent relaxation is seen to be an important first step towards the effects of residual stress on crack initiation and growth. The strain history, either tensile or compressive) of the weld region and its effect on material damage, cracking properties and creep damage development is seen as the key mechanism that needs to be understood and mechanistically explained. There is a need to highlight and resolve some of the problems associated with weldments and residual stresses before a comprehensive answer can be found. Development work on the improvement of testing, analysis and modelling as described in this paper could help in the future improvement of lifing methods of welded components.

References

AFCEN, "Design and construction rules for mechanical components of FBR nuclear islands,"

RCC-MR, Appendix A16, AFCEN, Paris.,1985.

API RP 579, 'Standardized fitness-for-service assessment techniques for pressurized equipment used in the petroleum industry', API, 2004.

ASME Boiler and Pressure Vessel Code (1991), Case N-47 (29), Class 1 components in elevated temperature service, Section III, Division I, ASME, New York.

ASTM E 1457-01, 2001, "Standard Test Method for Measurement of Creep Crack Growth Rates in Metals", ASTM Standards 03.01.

ASTM E647-99, 'Standard test method for measurement of fatigue crack growth rates', ASTM 2000, 03-01, 591-630.

BS7910,"Guide on methods for assessing the acceptability of flaws in fusion welded structures," London, BSI, 2000.

'CCG in C-Mn', 'CCG in Carbon-Manganese at 320-400', Brite/Euram project, 1993-1997.

'CRETE', 'Creep Crack Growth Testing for an EU CoP' , Brite/Euram project 2001-2004.

FITNET, 'Fitness for service analysis of structures using the FITNET procedure; An Overview', 24th Int. Conf. on Offshore Mechanics and Artic Eng., Greece 12-17 June 2005.

'HIDA', 'High Temperature Defect Assessment' Brite/Euram project, 1996-2000.

'LICON', 'Accelerated Test Methods for Advanced Steels' Brite/Euram project, 1997-2001.

'SINTAP', 'Structural integrity assessment procedures for European Industry', Brite/Euram.

R5-British Energy, "Defect assessment code of practice for High temperature metallic components," British Energy Generation Ltd. 2000.

R6, Assessment of the integrity of structures containing defects, Revision 3, British Energy Generation, 2000.

RCC-MR (1985) Technical Appendix A3, Section 1, Subsection Z, Materials design and construction rules for mechanical components of FBR nuclear test islands, AFCEN, Paris.

VAMAS TWA25, Code of Practice, ISO/TTA draft, ' Creep/fatigue Crack Growth in Components', VAMAS document, Ed. K. Nikbin, May 2005.

Bettinson, A.D., O'dowd, N.P., Nikbin, K. M., and Webster, G. A., (2002) 'Experimental Investigation of Constraint Effects on Creep Crack Growth', in PVP- Vol. 434, Computational Weld Mechanics, Constraint and Weld Fracture, ASME 2002, F.W. Brust, Ed., ASME New York, NY 10016, 143-150.

Davies, C. M., Dean, D. W., Nikbin, K. M., O'Dowd, N. P., (2006) 'Interpretation of Creep Crack Initiation and Growth Data for Weldments', WELDS05 Conference, GKSS Hamburg, Sept. 2005, Submitted to *the Eng. Fract. Mech. J.*, Dec. 2006.

Davies, C. M., Kourmpetis, M., O'Dowd, N. P. and Nikbin, K. M., (2006) 'Experimental Evaluation of the J or C* Parameter for a Range of Cracked Geometries', to be published in ASTM STP 1480.

Davies, C. M., Mueller, F., Nikbin, K. M., O'Dowd, N. P. and Webster, G. A., (2006) 'Analysis of Creep Crack Initiation and Growth in Different Geometries for 316H and Carbon Manganese Steels', to be published in ASTM STP 1480.

Dogan, B., Ceyhan, U., Nikbin, K., Petrovski, B., Dean, D.W., (2006) 'European Code of Practice for Creep Crack Initiation and Growth Testing of Industrial Specimens', to be published in ASTM STP 1480.

Lee, H.Y., Biglari, F., Wimpory, R., O'Dowd, N.P., Nikbin, K.M., (2004) "Treatment of residual stresses in life assessment procedures," Submitted to *ASTM international Journal*.

Lee, H. Y., Nikbin, K. M., (2005) 'Modelling the Redistribution of Residual Stresses in Components at Elevated Temperatures', ASTM STP 1480, to be published in the *Int. J. of ASTM*.

Nikbin, K., (2001) 'A unified European approach to high temperature defect assessment code and its incorporation in a knowledge base system', *Int. J. PVP*, pp. 929-935.

Nikbin, K.M., Smith, D.J. and Webster, G.A., (1984) 'Prediction of creep crack growth from uni-axial creep data', *Proc. Roy. Soc.* A.396,

183-197.

Nikbin, K.M., Smith, D.J. and Webster, G.A., (1986) 'An engineering approach to the prediction of creep crack growth', *J. Eng. Mat.* and *Tech., Trans ASME*, 108, 186-191.

O'Dowd, N.P., Nikbin, K.M., Biglari, F. R., (2005) in Proceedings of PVP 2005, ASME Pressure Vessels and Piping Division Conference July 17–21, Denver, Colorado USA, ISBN 0-7918-3763-7,I730CD.

O'Dowd, N.P., Nikbin, K.M., Lee, H-Y., Wimpory, R. and Biglari, F., (2004) "Stress Intensity Factors due to residual stresses in T-plate welds," *J PVT, ASME*, Vol. 126.

O'Dowd, N.P., Nikbin, K.M., Wimpory, R. C, Biglari, F. R. and O'Donnell, M. P. (2006) "Computational and experimental studies of high temperature crack growth in the presence of residual stress", in Proceedings of PVP 2006, Vanvouver.

Raju, I. S. and Newman, J. C., (1982) 'Stress-Intensity Factors for Internal and External Surface Cracks in Cylindrical Vessels'; *Journal of Pressure Vessel Technology*; Vol. 104: pp. 293-298.

Saxena, A., (1998) 'Non-linear fracture mechanics for engineers' CRC Press, Boca Raton, USA.

Tan, M., Célard, N. J. C., Nikbin, K. M and Webster, G. A., (2001) 'Comparison of Creep Crack Initiation and Growth in Four Steels Tested in HIDA', *International Journal of Pressure Vessels and Piping*, 78(12), pp. 737-747.

Turski M., Sherry, A.H, Bouchard, P.J. and Withers, P.J., (2004) *J. Neutron Research* **12**, 45–49.

Wasmer, K., Nikbin, K. M., Webster, G. A., (2004) "Sensitivity of Creep Crack Initiation and Growth in Plates to Material Properties Variations", Fatigue and Fracture Mechanics, ASTM STP 1461, Vol: 34, S. R. Daniewicz, J. C. Newman and K.-H. Schwalbe, Eds., ASTM International, West Conshohocken, PA.

Webster, G.A. and Ainsworth R.A., (1994) 'High temperature components life assessment' Chapman and Hall, London.

Webster, G. A, Nikbin, K. M., Chorlton, M. R.,

Célard, N. J. C. and Ober, M., (1998) 'Comparison of High Temperature Defect Assessments Methods'; *Material at High Temperature*; Vol. 15: pp. 337-346.

Wimpory, R.C., Biglari, F. R., Schneider, R., Nikbin, K. M. and O'Dowd, N.P., 2006 "Effect of residual stress on high temperature deformation in a weld stainless steel", ECRS7, Berlin.

Winstone, M.R., Nikbin, K.M. and Webster, G.A., (1985) 'Modes of failure under creep/fatigue loading of a nickel-based superalloy', *J. Mat. Sci.*, 20, 2471-2476.